This is a preprint, the final version is subject to change, of the American Mineralogist (MSA)
Cite as Authors (Year) Title. American Mineralogist, in press.
DOI: https://doi.org/10.2138/am-2020-7212

Experimental Determination of Solubility Constant of Kurnakovite, $MgB_3O_3(OH)_5 \bullet 5H_2O$

Yongliang Xiong[1]

Nuclear Waste Disposal Research & Analysis
Sandia National Laboratories
1515 Eubank Boulevard SE,
Albuquerque, NM 87123, USA

[1] Corresponding author, e-mail: yxiong@sandia.gov.

ABSTRACT

In this study, I present experimental results on the equilibrium between boracite [$Mg_3B_7O_{13}Cl(cr)$] and kurnakovite [chemical formula, $Mg_2B_6O_{11}\bullet15H_2O(cr)$; structural formula, $MgB_3O_3(OH)_5\bullet5H_2O(cr)$;] at 22.5 ± 0.5°C from a long-term experiment up to 1,629 days, approaching equilibrium from the direction of supersaturation,

$$Mg_3B_7O_{13}Cl(cr) + H^+ + 2B(OH)_4^- + 18H_2O(l) \rightleftharpoons 3MgB_3O_3(OH)_5\bullet5H_2O(cr) + Cl^-$$

Based on solubility measurements, the 10-based logarithm of the equilibrium constant for the above reaction at 25°C is determined to be 12.83 ± 0.08 (2σ).

Based on the equilibrium constant for dissolution of boracite,

$$Mg_3B_7O_{13}Cl(cr) + 15H_2O(l) = 3Mg^{2+} + 7B(OH)_4^- + Cl^- + 2H^+$$

at 25°C measured previously (Xiong et al., 2018) and that for the reaction between boracite and kurnakovite determined here, the equilibrium constant for dissolution of kurnakovite,

$$MgB_3O_3(OH)_5\bullet5H_2O(cr) = Mg^{2+} + 3B(OH)_4^- + H^+ + H_2O(l)$$

is derived as -14.11 ± 0.40 (2σ).

Using the equilibrium constant for dissolution of kurnakovite obtained in this study and the experimental enthalpy of formation for kurnakovite from the literature, a set of thermodynamic properties for kurnakovite at 25°C and 1 bar is recommended as follows: ΔH_f^0 = –4813.24 ± 4.92 kJ•mol^{-1}, ΔG_f^0 = –4232.0 ± 2.3 kJ•mol^{-1}, and S^0 = 414.3 ± 0.9 J•mol^{-1}•K^{-1}. Among them, the Gibbs energy of formation is based on the equilibrium constant for kurnakovite determined in this study; the enthalpy of formation is from the literature, and the standard entropy is calculated internally with the Gibbs-Helmholtz equation in this work. The thermodynamic properties of kurnakovite estimated using the group contribution method for borate minerals based on the sum of contributions from the cations, the borate polyanions, and the structural water to the thermodynamic properties from the literature, are consistent, within its uncertainty, with the values listed above.

Since kurnakovite usually forms in salt lakes rich in sulfate, studying the interactions of borate with sulfate is important to modeling kurnakovite in salt lakes. For this purpose, I have re-calibrated our previous model (Xiong et al., 2013) describing the interactions of borate with sulfate based on the new solubility data for borate in Na_2SO_4 solutions presented here.

INTRODUCTION

Kurnakovite, which has a structural formula of $MgB_3O_3(OH)_5•5H_2O$(cr)(“cr” refers to “crystalline”, thereafter), is a magnesium borate mineral of triclinic symmetry in the space group of $P\bar{1}$. In kurnakovite, there are the following structural units: triangularly-coordinated [$BO_2(OH)$]-groups, tetrahedrally-coordinated [$BO_2(OH)_2$]-

groups, and $Mg(OH)_2(H_2O)_4$ octahedra, connected into neutral $Mg(H_2O)_4B_3O_3(OH)_5$ units forming chains along the [001] direction (Gatta et al., 2019). The mineral that has the same chemical composition but is of monoclinic symmetry is called inderite. Kurnakovite was discovered by Godlevsky (1940) in the borate deposits of west Kazakhstan. Rumanova and Ashirov (1964) determined its densities and refractive indices. Then, Yeh (1965) did some crystal structure determinations for kurnakovite. Razmanova et al. (1970) solved its structure, and Corazza (1974) made a refinement for the structure. Zhou et al. (2012a) refined the hydrogen positions using nuclear magnetic resonance (NMR). Most recently, Gatta et al. (2019) studied the crystal structure and chemistry of a natural kurnakovite from Kramer Deposit, California, using single-crystal neutron diffraction. Kurnakovite was synthesized by Spiryagina (1949) and Yuan et al. (1983). Heinrich (1946) also synthesized kurnakovite, corresponding to the occurrence in USA, but it seems that he mislabeled it as inderite, as Frondel et al. (1956) did (Schaller and Mrose, 1960) (see below).

The currently available thermodynamic properties of kurnakovite are inconsistent. Li et al. (1997) measured its enthalpy of formation, and Li et al. (2000) estimated its Gibbs energy of formation as -4249.79 $kJ \bullet mol^{-1}$. By contrast, Anovitz and Hemingway (2002) estimated its Gibbs energy of formation as -4272 $kJ \bullet mol^{-1}$, differing the estimated value from Li et al. (2000) by ~23 $kJ \bullet mol^{-1}$. Therefore, its Gibbs free energy of formation is not well known, leading to the inexact knowledge of its solubility constant. In this work, the solubility constant of kurnakovite is determined to provide a set of its thermodynamic properties.

Given the occurrence of kurnakovite in sulfate-enriched salt lakes in nature, Xiong et al. (2013) developed a model to describe the interactions between sulfate and borate based on literature data on the solubility of sodium tetraborate (borax) in Na_2SO_4 solutions without any pH measurements. In the present work, the previous model has been recalibrated to describe the important interactions between sulfate and borate for modeling the formation of kurnakovite in sulfate-enriched salt lakes in nature, based on our own borax solubility data together with pH measurements in Na_2SO_4 solutions up to 1.8 mol•kg^{-1}.

OCCURRENCE OF KURNAKOVITE

Kurnakovite has been reported from about 12 localities worldwide, including the type locality in the gypsum cap of the Inder salt dome, Kazakhstan. In USA, it is present in the Jennifer Mine of the Kramer borate deposit, Kern County (Frondel et al., 1956; Schaller and Mrose, 1960; Pemberton, 1983) (however, Frondel et al. mislabeled kurnakovite as inderite, according to Schaller and Mrose, 1960 and Baysal, 1973), and in the Furnace Creek district, Inyo County (Erd et al., 1970), California. In Turkey, it is present in the Kirka borate deposit (Baysal, 1973; Inan et al., 1973; Helvaci, 1978). In China, it occurs in Da Qaidam Lake and Xiao Qaidam Lake (Qian and Xuan, 1985; Zheng et al., 2005; Li et al., 2012; Li et al., 2013), the Yashatu deposit (Jiang et al., 1996), Qinghai Province; in Zhacang Chaka Salt Lake (Zheng and Liu, 1982; Yang and Zheng, 1985), Nie'er Cuo Salt Lake (Yang and Zheng, 1985; Liu and Zheng, 2010), Chala Ka Salt Lake (Yang and Zheng, 1985), Qag Caca Salt Lake (Yang, 1991), and Jibu

Salt Lake (Li et al., 2004), Xizang (Tibet) Autonomous Region. In Argentina, it occurs in the Tincalayu borax mine, Salta (Hurlbut and Erd, 1974).

At several of these localities, kurnakovite commonly forms in current salt lakes that are rich in sulfate (Sun et al., 1984; Yang, 1989; Yuan et al., 1993; Liu et al., 2003; Zheng and Liu, 2009), and formed in ancient or extinct salt lakes that were also rich in sulfate such as those Neogene salt lakes in the western Turkey (Kistler and Helvacı, 1994) and those Miocene-Pliocene salt lakes in the Death Valley, California, USA (Erd et al., 1970; Tanner, 2002), as evidenced by the occurrence of both kurnakovite and gypsum in those Neogene and Miocene-Pliocene deposits such as the Kirka borate deposit (Helvaci et al, 1993) and the borate deposits in the Furnace Creek Formation in the Death Valley (Erd et al., 1970; Tanner, 2002).

PRACTICAL APPLICATIONS OF KURNAKOVITE

Kurnakovite has several practical applications. In the oil and gas industry, kurnakovite is one of the borate minerals used in the hydrofracturing fluids as cross-linkers for extraction of shale gas (Dobson et al., 2005). This usage is based on the fact that kurnakovite is a sparingly soluble borate mineral. Kurnakovite is used for neutron shielding (Senberber et al., 2017; Gatta et al., 2019), as kurnakovite has the lowest neutron radiation permeability among the common borate minerals (Derun and Kipcak, 2011). Kurnakovite also has interesting luminescence properties with its excitation spectrum at 360 nm and emission spectrum at 420 nm (Yuan et al., 1993). In the field of nuclear waste management, sparingly soluble borate minerals may impact the near-field chemistry of geological repositories, because sparingly soluble borate minerals may have an impact on aqueous geochemistry of near-field environments as solubility-controlling phase(s) for borate in geological repositories. This is especially true with geological repositories in salt formations. Salt formations are considered to be ideal for nuclear waste isolation (National Academy of Science's Committee on Waste Disposal, 1957), and there are relatively high concentrations of borate present in brines associated with salt formations (e.g., up to 0.18 mol•kg^{-1}, Xiong and Lord, 2008). As borate could potentially form an aqueous complex with Am(III) (Borkowski et al., 2010; Xiong, 2017), the formation of sparingly soluble borate minerals in the near-field of a geological repository could keep borate concentrations low, minimizing the contributions of the aqueous Am(III)-borate complex to the solubility of Am(III).

EXPERIMENTAL METHODS

Solubility measurements were performed from the direction of supersaturation, similar to the approach we used before for the determination of solubility constants of boracite [$Mg_3B_7O_{13}Cl$(cr)] and aksaite [$MgB_6O_7(OH)_6•2H_2O$(cr)] (Xiong et al., 2018). The experimental products were not sampled until after the experiment had run for at least 957 days. All chemicals used in our experiment were ACS reagent grade. The solutions used in the experiments were prepared from the degassed deionized (DI) water with resistivity ≥ 18.2 megohm in which any dissolved CO_2 was removed, according to the procedure of Wood et al. (2002).

Our experiments with regard to solubility measurements for borax in Na_2SO_4 solutions from undersaturation are similar to our previous work in NaCl solutions (Xiong et al., 2013).

The pH readings were measured with an Orion-Ross combination pH glass electrode, coupled with an Orion Research EA 940 pH meter that was calibrated with three pH buffers (pH values: 4, 7, and 10). Negative logarithms of hydrogen-ion concentrations on molar scale (pcH) were determined from pH readings by using correction factors (Hansen, 2001). Based on the equation in Xiong et al. (2010), pcHs are converted to negative logarithms of hydrogen-ion concentrations on molal scale, pH_m, a notation from Oak Ridge National Laboratory/University of Idaho (e.g., Wood et al., 2002).

Solution samples were periodically withdrawn from experimental runs. Before solution samples were taken, pH readings of experimental runs were first measured. The sample size was usually 3 mL. After a solution sample was withdrawn from an experiment and filtered with a 0.2 μm syringe filter, the filtered solution was then weighed, acidified with 0.5 mL of concentrated TraceMetal® grade HNO_3 from Fisher Scientific, and finally diluted to a volume of 10 mL with DI water. If subsequent dilutions were needed, aliquots were taken from the first dilution samples for the second dilution, and aliquots of the second dilution were then taken for the further dilution.

Boron, sodium and magnesium concentrations of solutions were analyzed with a Perkin Elmer dual-view inductively coupled plasma-atomic emission spectrometer (ICP-AES) (Perkin Elmer DV 8300). Calibration blanks and standards were precisely matched with experimental matrices. The linear correlation coefficients of calibration curves in all measurements were better than 0.9995. The analytical precision for ICP-AES is better than 1.00% in terms of the relative standard deviation (RSD) based on replicate analyses.

Chloride concentrations were analyzed with a DIONEX ion chromatograph (IC) (DIONEX IC 3000).

The solid phase identification was performed using a Bruker AXS, Inc., D8 Advance X-ray diffractometer (XRD) with a Sol-X detector. XRD patterns were collected using CuKα radiation at a scanning rate of 1.33^o/min for a 2θ range of 10–90^o.

EXPERIMENTAL RESULTS

Figure 1 shows the XRD patterns of solid phases from my supersaturation experiment with an initial concentration of 1.0 mol•kg^{-1} $MgCl_2$ solution. Figure 1 shows that kurnakovite along with boracite and aksaite crystallized from the solution. Notice that the peaks characteristic of kurnakovite and boracite, are present in the XRD patterns (Figure 1). In our previous work, we determined the thermodynamic properties of boracite and aksaite (Xiong et al., 2018).

Experimental results from the direction of precipitation of kurnakovite are tabulated in Table 1. In Figure 2, total boron, chloride, magnesium and sodium concentrations as a function of experimental time are displayed. As shown in Figure 2, the equilibrium was established after about 900 days. The duration of the experiment was up to 1,642 days (Table 1, Figure 2).

In Table 2, solubility data of borax in Na_2SO_4 solutions at 25 ^oC are presented. The experimental time was up to 762 days. The experimental duration for these experiments is similar to that for our previous solubility measurements of borax in NaCl solutions, which was 567 days (Xiong et al., 2013), and to that for our previous solubility study of borax in a 0.01 mol•kg^{-1} $MgCl_2$ solutions (Xiong et al., 2017). In our previous studies, we demonstrated that the equilibrium for solubility of borax was attained after ~130 days. Therefore, based on our previous studies, it is assumed that the equilibrium was attained for solubility of borax in Na_2SO_4 solutions in this study.

THERMODYNAMIC CALCULATIONS AND DISCUSSION

In our previous work, we determined the thermodynamic properties of boracite and aksaite (Xiong et al., 2018).

The equilibrium between boracite and kurnakovite can be represented by the following reactions,

$$Mg_3B_7O_{13}Cl(cr) + H^+ + 2B(OH)_4^- + 18H_2O(l) \rightleftharpoons 3MgB_3O_3(OH)_5{\bullet}5H_2O(cr) + Cl^- \quad (1)$$

Regarding Reaction (1), its equilibrium constant at infinite dilution can be expressed as follows,

$$K_1^0 = \frac{(a_{Cl^-})}{(a_{H^+})\times(a_{B(OH)_4^-})^2\times(a_{H_2O})^{18}} \quad (2)$$

In Equation (1), a_i is an activity of the i-th species calculated with a thermodynamic model; a_{H_2O} is the activity of water.

Activities of $B(OH)_4^-$, Cl^-, H^+ and water in the experimental system are calculated using the computer code EQ3/6 Version 8.0a (Wolery et al., 2010; Xiong, 2011a). The database used for calculations was DATA0.FM2 (Domski, 2015; Xiong and Domski, 2016).

Based on the activities calculated using EQ3/6 Version 8.0a, the $\log_{10} K_1^0$ at infinite dilution is calculated in accordance with Equation (2) (Table 3). The equilibrium constant for $\log_{10} K_1^0$ obtained in this study is 12.83 ± 0.08 (2σ).

The dissolution reaction for kurnakovite can be expressed as follows,

$$MgB_3O_3(OH)_5\bullet 5H_2O(cr) = Mg^{2+} + 3B(OH)_4^- + H^+ + H_2O(l) \qquad (3)$$

The equilibrium constant for Reaction (3) can be derived from $\log_{10} K_1^0$ for Reaction (1) and $\log_{10} K_4^0$ for Reaction (4) regarding dissolution of boracite,

$$Mg_3B_7O_{13}Cl(cr) + 15H_2O(l) = 3Mg^{2+} + 7B(OH)_4^- + Cl^- + 2H^+ \qquad (4)$$

The equilibrium constant for Reaction (4) ($\log_{10} K_4^0$) has been determined as -29.50 ± 0.39 (2σ) by solubility measurements (Xiong et al., 2018). That value is in excellent agreement with a value calculated from the ΔG_f^0 for boracite from the literature (Khodakovsky, Semenov and Aksaenova, unpublished, see citation in Anovitz and Hemingway, 2002, and discussion in Xiong et al., 2018).

According to $\log_{10} K_1^0$ for Reaction (1) determined in this study and $\log_{10} K_4^0$ for Reaction (4) from Xiong et al. (2018), the equilibrium constant for Reaction (3) ($\log_{10} K_3^0$) is derived as –14.11 ± 0.40 (2σ) (Table 3).

The equilibrium constant for kurnakovite determined by this study provides an opportunity in evaluating the Gibbs free energies of this phase from the estimates in the literature. In the group contribution method, the thermodynamic properties for a borate phase are sum of contributions from the cations in aqueous solution, the borate polyanions, and the structural water to the corresponding thermodynamic properties (Li et al., 2000). Li et al. (2000) calculated the ΔG_f^0 of kurnakovite as –4249.79 kJ•mol^{-1}, according to the group contribution method. Based on this value, $\log_{10} K_3^0$ for Reaction (3) is calculated to be –17.23 (Table 4). Anovitz and Hemingway (2002) estimated the ΔG_f^0 of kurnakovite as –4272 kJ•mol^{-1}, leading to a value of –21.16 for $\log_{10} K_3^0$ for Reaction (3) (Table 4). In comparison with the value determined in this study [–14.11 ± 0.40 (2σ)], the value (–17.23) calculated based on the group contribution method (Li et al., 2000) is off by about three orders of magnitude. This is reasonable considering the accuracy of the group contribution method in estimation of ΔH_f^0 and ΔG_f^0 (see below). In contrast, the value (–21.16) estimated from the method of Anovitz and Hemingway (2002) is off by about seven orders of magnitude. The estimation method of Anovitz and Hemingway (2002) is similar to the methods proposed by Robinson and Haas (1983) and Chermak and Rimstidt (1989) for silicate minerals. Therefore, the group contribution method of Li et al. (2000) performs better than the estimation method of Anovitz and Hemingway (2002). This finding is similar to our previous observation with regard to aksaite (Xiong et al., 2018).

According to $\log_{10} K_3^0$ for Reaction (3) from this work, the ΔG_f^0 for kurnakovite is derived as –4231.95 ± 2.29 kJ•mol^{-1} (Table 5). Li et al. (2000) calculated the ΔG_f^0 for kurnakovite as –4249.79 kJ•mol^{-1}, which deviates from my ΔG_f^0 by –17.84 kJ•mol^{-1}, indicating that the error associated with the calculation of Li et al. (2000) is 0.42% in terms of ΔG_f^0. This error is within the error range, 0.01-0.60%, for the group contribution method (Li et al., 2000). They also calculated the ΔH_f^0 of kurnakovite as -4831.81 kJ•mol^{-1}. The experimentally determined ΔH_f^0 of kurnakovite is –4813.24 kJ•mol^{-1}. Therefore, the calculated ΔH_f^0 deviates from the experimental value by –18.57 kJ•mol^{-1}, almost identical to the difference between the calculated and experimental ΔG_f^0's.

If we use the calculated values as the benchmarks, the above identical differences in comparing the calculated and experimental values demonstrate that our experimentally derived ΔG_f^0 is highly consistent with the experimental ΔH_f^0 from Li et al. (1997). To state in a different way, the difference between the calculated ΔH_f^0 and ΔG_f^0 is –582.02 kJ•mol^{-1}. Interestingly, the difference between the experimental ΔH_f^0 of Li et al. (1997) and my experimentally derived ΔG_f^0 is –581.29 kJ•mol^{-1}, which is almost identical to the above difference for the calculated ΔH_f^0 and ΔG_f^0.

Regarding the entropy of kurnakovite, the value derived by this study from the experimental ΔG_f^0 and ΔH_f^0 is 414.31 J•mol^{-1}•K^{-1}, which carries an uncertainty of ~1 J•mol^{-1}•K^{-1}. The entropy calculated internally with the Gibbs-Helmholtz equation by this study based on the estimated ΔG_f^0 and ΔH_f^0 from Li et al. (2000) is 411.85 J•mol^{-1}•K^{-1}. As the calculated ΔG_f^0 and ΔH_f^0 from Li et al. (2000) do not have error estimates, there is no error estimate on the entropy calculated here. Taking into consideration the uncertainties associated with the experimentally-derived entropy, and with the estimated entropy, the difference between these two entropies would be similar to those between experimentally-derived and estimated ΔG_f^0, and between experimentally-derived and estimated ΔH_f^0, and be within the error range for the group contribution method (i.e., to 0.6%).

It is noted that Birsoy and Özbas (2012) used a value of –4366.90 kJ•mol^{-1} for the Gibbs free energy of formation for kurnakovite in their calculations of activity diagrams of borates. They cited Anovitz and Hemingway (2002) as the source. In fact, the primary source for that value is from Huang et al. (1988). However, the enthalpy value (–4856 kJ•mol^{-1}) measured by Huang et al. (1988) is more negative than the valued (-4813.24 kJ•mol^{-1}) determined by Li et al. (1997). In addition, the entropy value (361. 7 J•mol^{-1}•K^{-1}) obtained by Huang et al. (1988) seems too low in comparison with the recent values (e.g., 405 J•mol^{-1}•K^{-1} from Anovitz and Hemingway, 2002; and 414.31 J•mol^{-1}•K^{-1} from this work).

In natural salt lakes such as those in the Qinghai-Xizhang (Tibet) Plateau, China, kurnakovite occurs in those lakes which are rich in borate and sulfate. Therefore, the interactions of borate with sulfate are important to modeling the formation of kurnakovite in salt lakes in nature. In our previous work (Xiong et al., 2013), we developed a model to describe the interactions between sulfate and borate based on the solubility data of borax in Na_2SO_4 solutions from the literature. However, the solubility data from the literature, used for development of our model, lacked pH measurements. In this work, we re-calibrate our model based on our solubility measurements on borax in Na_2SO_4 solutions with pH_m measurements (Table 2).

The parameters for the re-calibrated model are tabulated in Table 6. As indicated in Table 6, there are changes in the Pitzer parameters for the interactions of $B(OH)_4^-$—SO_4^{2-} and $B_4O_5(OH)_4^{2-}$—SO_4^{2-}—Na^+ in the re-calibrated model. The $\log_{10} K_{sp}^0$ for borax (sodium tetraborate decahydrate) from the re-calibrated model agrees with the previous value within the quoted uncertainties (Table 6).

In Figure 3, our experimental data in Na_2SO_4 solutions are compared with the values predicted by the re-calibrated model, by our previous model (Xiong et al., 2013), and by the model of Felmy and Weare (1986). Figure 3 indicates that our re-calibrated model performs well. Our previous model based on the literature data without pH measurements performs reasonably well. The model of Felmy and Weare (1986) seems to overpredict total boron concentrations as a function of ionic strength.

In Table 7, the predicted values for elemental concentrations using the previous model of Xiong et al. (2013), the recalibrated model presented in this work, and the Felmy and Weare (1986) model are compared with the experimental values for borax solubilities in the assemblage of halite+borax+nahcolite. Table 7 shows that the values predicted by the model of Xiong et al. (2013) and the re-calibrated model are in better agreement with the experimental values taken from Teeple (1929) than the Felmy and Weare (1986) model. Notice that the B(III) elemental concentration changes by using the re-calibrated model in this work with respect to the previous model by Xiong et al. (2013). The B(III) concentration predicted by the re-calibrated model is in excellent agreement with the experimental value.

Similarly, in Table 8, the values predicted by the previous model of Xiong et al. (2013), the recalibrated model presented in this work and the Felmy and Weare (1986) model are compared with the experimental values with the experimental values from Teeple (1929) for borax solubilities in the assemblage of borax+sodium pentaborate. Table 8 shows that the values predicted by the model of Xiong et al. (2013) and the re-calibrated model are in excellent agreement with the experimental values, whereas those predicted by the Felmy and Weare (1986) model are off.

In our model developed in 2013 (Xiong et al., 2013), we first introduced $NaB(OH)_4(aq)$ into the borate model to accurately describe the interaction between borate and sodium, as various techniques including the vapor pressure method, conductivity measurements, and dielectric spectroscopy indicate the presence of $NaB(OH)_4(aq)$ (Rowe and Atkinson, 1990; Weres, 1995; Buchner et al., 1999). The advances in borate chemistry since then have further supported our addition of $NaB(OH)_4(aq)$ into the borate chemistry model. First, Zhou et al. (2012b) provided the clear structural evidence for the existence of $NaB(OH)_4(aq)$. Zhou et al. (2012b) used a rapid liquid X-ray diffractometry with a highly effective *X'celerator*® detector to investigate the diffusion structure of aqueous sodium borate solutions at 25 ^{o}C. They found out that the free Na^+ and $B(OH)_4^-$ ions combine to form contact ion pair (CIP), $NaB(OH)_4(aq)$. Zhou et al. (2017) further

DOI: https://doi.org/10.2138/am-2020-7212

studied the association of $B(OH)_4^-$ with Na^+ via the X-ray diffraction technique with the empirical potential structure refinement (EPSR) modeling. In addition, Zhou et al. (2017) performed Density Function Theory (DFT) calculations for the structure and stability of $NaB(OH)_4(aq)$. Their work further demonstrates that Na^+ and B forms contact ion pair. Second, the most recent conductivity measurements by Arcis et al. (2016) also confirm the existence of $NaB(OH)_4(aq)$.

The contributions of $NaB(OH)_4(aq)$ to total borate concentrations are expected to be significant in Na-rich solutions. As illustrated by Table 9, the predicted concentrations of $NaB(OH)_4(aq)$ to the total borate concentrations for the assemblage of borax and mirabilite ($Na_2SO_4{\bullet}10H_2O$) at 25°C are 16 % (based on the model of Xiong et al., 2013) or 11% (based on the recalibrated model in this work).

IMPLICATIONS

As borate can form an aqueous complex with actinides(III), an immediate implication is that the formation of magnesium-bearing borates such as kurnakovite will minimize the concentrations of the aqueous actinides(III)-borate complex to the solubility of actinides(III), by sequestrating soluble borate. This is because the brines in salt formations commonly contain high concentrations of magnesium. For instance, the magnesium concentration in the Generic Weep Brine (GWB) at the Waste Isolation Pilot Plant (WIPP), a geological repository for transuranic waste in the southeastern New Mexico, USA, is 1.16 $mol \cdot kg^{-1}$ (Xiong and Lord, 2008).

Another important implication from this study is that our thermodynamic model can accurately describe the interactions between borate and sulfate. Therefore, our model can be applied to salt lakes with high concentrations of sulfate for efficient recovery of borate.

Finally, as kurnakovite has important industrial applications, the thermodynamic model presented in this study for kurnakovite could increase its usefulness, because the model can be applied to optimize crystallization of kurnakovite from natural brines and its synthesis on an industrial scale.

It is of interest to note that the *ab-initio* calculations have been attempted for assessment of thermodynamic properties of the aqueous species of some heavy metals (Vetuschi Zuccolini et al., 2011). Therefore, it will be valuable to apply *ab-initio* calculations to the borate system including solid boron phases and aqueous borate species in the future. When that happens, it will be possible to compare the *ab-initio* calculations with the empirical estimation methods such as the group contribution method for borates from Li et al. (2000) and the method of Anovitz and Hemingway (2002) for borates, which adopted the methodology for silicates, against the bench-mark experimental values. It would also provide new insights into the speciation scheme of aqueous borate species.

ACNOWLEDGEMENTS

Sandia National Laboratories is a multi-mission laboratory operated by National Technology and Engineering Solutions of Sandia, LLC., a wholly owned subsidiary of Honeywell International, Inc., for the U.S. Department of Energy's National Nuclear Security Administration under contract DE-NA-0003525. SAND2019-4805J. This paper describes objective technical results and analysis. Any subjective views or opinions that might be expressed in the paper do not necessarily represent the views of the U.S. Department of Energy or the United States Government. The author thanks two journal reviewers, the Associate Editor, Professor Edward Grew, for their thorough and insightful reviews, which significantly improved the presentation. The editorial efforts by the Editor, Dr. Hongwu Xu, are gratefully acknowledged. The author is grateful to the following colleagues and student interns for the laboratory assistance: Leslie Kirkes, Terry Westfall, Cassie Marrs, Jandi Knox, Heather Burton, Diana Goulding, Brittany Hoard, Chase Kicker, Danelle Morrill, Rachael Roselle, Mathew Stroble, William Sullvan, Kira Vicent, and Yoni Xiong.

DOI: https://doi.org/10.2138/am-2020-7212

REFERENCES

Anovitz, L.M., and Hemingway, B.S. (2002) Thermodynamics of boron minerals: Summary of structural, volumetric and thermochemical data. In Grew, E.S., and Anovitz, L.M., Editors, Boron: Mineralogy, Petrology, and Geochemistry, Reviews in Mineralogy, Volume 33, p. 181-262, .2nd Printing, Mineralogical Society of America, Washington, D.C., USA.

Arcis, H., Ferguson, J.P., Zimmerman, G.H. and Tremaine, P.R. (2016) The limiting conductivity of the borate ion and its ion-pair formation constants with sodium and potassium under hydrothermal conditions. Physical Chemistry Chemical Physics, 18, 24081–24094.

Baysal, O. (1973) New hydrous magnesium-borate minerals in Turkey: kurnakovite, inderite, inderborite. Bull. Min. Res. & Explor. Inst. Ankara, 80, 93–103.

Birsoy, R. and Özbaş, Ü. (2012) Activity diagrams of borates: implications on common deposits. Carbonates and evaporites, 27, 71–85.

Borkowski, M., Richmann, M., Reed, D.T., and Xiong, Y.-L. (2010) Complexation of Nd(III) with Tetraborate Ion and Its Effect on Actinide (III) Solubility in WIPP Brine. Radiochimica Acta, 98, 577–582.

Braitsch, O. (1971) Other Components of Salt Deposits. In *Salt Deposits: Their Origin and Composition* (pp. 215-245). Springer Berlin Heidelberg.

Buchner, R., Hefter, G., May, P., and Sipos, P. (1999) Dielectric relaxation of dilute aqueous NaOH, $NaAl(OH)_4$, and $NaB(OH)_4$. Journal of Physical Chemistry, B 103, 11186–11190.

Chermak, J.A., and Rimstidt, J.D. (1989) Estimating the thermodynamic properties (ΔG_f^0 and ΔH_f^0) of silicate minerals at 298 K from the sum of polyhedral contributions. American Mineralogist, 74, 1023–1031.

Corazza, E. (1974) The crystal structure of kurnakovite: a refinement. Acta Crystallographica Section B: Structural Crystallography and Crystal Chemistry, 30, 2194–2199.

Derun, E. and Kipcak, A. (2011) Characterization of some boron minerals against neutron shielding and 12 year performance of neutron permeability. Journal of Radioanalytical and Nuclear Chemistry, 292, 871-878.

Dobson Jr, J.W., Hayden, S.L. and Hinojosa, B.E., Texas United Chemical Corp (2005) *Borate crosslinker suspensions with more consistent crosslink times*. U.S. Patent 6,936,575.

Domski, P.S. (2015) "Memo AP-173, EQ3/6 Database Update: DATA0.FM2" Memorandum to WIPP Records, October 27, 2015. Carlsbad, NM: Sandia National Laboratories. ERMS 564914.

Erd, R. C., McAllister, J. F., Vlisidis, A.C. (1970) Wardsmithite, $5CaO{\bullet}MgO{\bullet}12B_2O_3{\bullet}30H_2O$, a new borate mineral from the Death Valley region, California, American Mineralogist, 55, 349–357.

Felmy, A.R., Weare, J.H. (1986) The prediction of borate mineral equilibria in natural waters: Applications to Searles Lake, California. Geochimica et Cosmochimica Acta, 50, 2771–2783.

Frondel, C., Morgan, V. and Waugh, J.L.T. (1956) Lesserite, A new borate mineral. American Mineralogist, 41, 927–928.

Gatta, G.D., Guastoni, A., Lotti, P., Guastella, G., Fabelo, O. and Fernandez-Diaz, M.T. (2019) A multi-methodological study of kurnakovite: A potential B-rich aggregate. American Mineralogist, 104, 1315–1322.

Godlevsky, M.N. (1940) Kurnakovite, a new borate. Compt. Rend. Doklady Acad. Sci., U.S.S.R., 28, 638–640).

Hansen, D.J. (2001) Determining aluminum solubilities as part of cement degradation studies in support of the Waste Isolation Pilot Plant. SAND2001-2144P, Albuquerque, NM: Sandia National Laboratories.

Heinrich, E. W. (1946), A second discovery of inderite: American Mineralogist, 31, 71–76.

Helvaci, C. (1978) A review of the mineralogy of the Turkish borate deposits. Mercian Geology, 6(4), 257–270.

Helvacı, C., Stamatakis, M.G., Zagouroglou, C. and Kanaris, J. (1993) Borate minerals and related authigenic silicates in northeastern Mediterranean late Miocene continental basins. Exploration and Mining Geology, 2, 171–178.

Huang, S., Zhang, Q., Li, Y. And Chen, P. (1988) The specific heat measurements of kurnakovite ($2MgO{\bullet}3B_2O3{\bullet}15H_2O$) from 65 to 310K and calculation of its thermodynamic properties. Acta Chimica Sinica, 46, 967–971.

Hurlbut, C. S., Erd, R. C. (1974) Aristarainite, $Na_2O{\bullet}MgO{\bullet}6B_2O_3{\bullet}10H_2O$, a new mineral from Salta, Argentina, American Mineralogist, 59, 647–651.

Jiang, C., Zheng, M., Wang, P. Qian, Y., and Liao, D. (1996) Chapter 21. Boron Deposits of China. In Editorial Committee of the Mineral Deposits of China, Mineral Deposits of China, Volume 5, p. 1–51. Geological Publishing, Beijing, China.

Kistler, R.B. and Helvaci, C. (1994) Boron and borates. Industrial minerals and rocks, 6, 171–186.

Li, W.-Z, Zheng, M-P.. and Zhao, Y.-Y. (2004): The status and suggestions on the exploitation and application of magnesium-borate minerals in Tibet. Resources & Industries 6(5), 33-37 (in Chinese with English abstract).

Li, J., Gao, S., Xia, S., Li, B. and Hu, R. (1997) Thermochemistry of hydrated magnesium borates. The Journal of Chemical Thermodynamics, 29, 491–497.

Li, J., Li, B. and Gao, S. (2000) Calculation of thermodynamic properties of hydrated borates by group contribution method. Physics and Chemistry of Minerals, 27(5), 342-346.

Li, X., Liu, Z., Gao, S. and Xia, S. (2012) Geochemical hypothesis for hydrated magnesium borate deposit in Salt Lake, NW China. Environmental Earth Sciences, 66, 1431–1438.

Li, X., Gao, S., Liu, Z., and Xia, S. (2013) Kurnakovite deposits on the Qinghai-Tibet Plateau (II): An investigation from chemical kinetics of chloropinnoite dissolution. Environmental Earth Sciences, 70, 1151–1158.

Liu, X.F. and Zheng, M.P. (2010) Geological features and metallogenic mechanism of the Nieer Co magnesium borate deposit, Tibet. Acta Geologica Sinica, 84, 1601–1612.

Liu, Z.H., Hu, M.C., Gao, S.Y. and XIA, S.P. (2003) Experiment on formation process of kurnakovite and pinnoite. Geochimica, 32(6), 569–572.

National Academy of Science's Committee on Waste Disposal. 1957. *The Disposal of Radioactive Waste on Land*. Publication 519. Washington, DC: National Academy of Sciences–National Research Council.

Nies, N.P. and Hulbert, R.W. (1967) Solubility isotherms in the system sodium oxide-boric oxide-water. Revised solubility-temperature curves of boric acid, borax, sodium pentaborate, and sodium metaborate. Journal of Chemical and Engineering Data, 12, 303–313.

Pemberton, H.E. (1983) BMinerals of California. Van Nostrand, New York. 591 p.

Qian, Z. and Xuan, Z. (1985) Borate minerals in salt lake deposits at Chaidamu Basin, China. Sixth International Symposium on Salt, 1983, vol. 1, 185–192.

Razmanova, Z.P., Rumanova, I.M. and Belov, N.V. (1970) Crystal Structure of Kurnakovite $Mg_2B_6O11 \cdot 15H_2O = 2Mg [B_3O_3(OH)_5] \cdot 5H_2O$. In *Soviet Physics Doklady* (Vol. 14, p. 1139).

Robinson, G.R., Jr., Haas, J.L., Jr. (1983) Heat capacity, relative enthalpy, and calorimetric entropy of silicate minerals: An empirical method of prediction. American Mineralogist, 68, 541–553.

Rowe, L., Atkinson, G. (1990) The effect of pressure on the formation of alkali metal borate ion pairs at 25°C. Journal of Solution Chemistry, 19, 149–158.

Rumanova, I.M. and Ashirov, A. (1964) The determination of the crystal structure of inderite. Sov. Phys Cryst., 8, 414–428.

Schaller, W.T. and Mrose, M.E. (1960) The naming of the hydrous magnesium borate minerals from Boron, California - a preliminary note. American Mineralogist, 45, 732–734.

Senberber, F.T., Yildirim, M., Özdogan, I.N., Kipcak, A.S. and Derun, E. (2017) Dehydration behavior and kinetics of kurnakovite under microwave irradiation. Turkish Journal of Chemistry, 41, 399–409.

Spiryagina, A. (1949) Conditions of formation of kurnakovite. In *Dokl. Akad. Nauk SSSR* (Vol. 68).

Sun, D.-P., Gao, Z.-H., Wang, K.-J.(1984) The origins of borates in saline lakes, Qinghai-Xizaig plateau. Acta Sedimentologica Sinica, 2(4), 111–126.

Tanner, L.H. (2002) Borate formation in a perennial lacustrine setting: Miocene–Pliocene furnace creek formation, Death Valley, California, USA. Sedimentary Geology, 148, 259–273.

Teeple, J.E. (1929) *The industrial development of Searles Lake brines with equilibrium data*. The Chemical Catalog Company, Inc.; New York.

Vetuschi Zuccolini, M., Ottonello, G. and Belmonte, D. (2011) Ab-initio assessment of conventional standard-state thermodynamic properties of geochemically relevant gaseous and aqueous species. Computers & Geosciences, 37, 646–661.

Wagman, D.D., Evans, W.H., Parker, V.B., Schumm, R.H. and Halow, I. (1982) *The NBS tables of chemical thermodynamic properties. Selected values for inorganic and C1 and C2 organic substances in SI units*. National Standard Reference Data System.

Weres, O. (1995) Vapor pressure, speciation, and chemical activities in highly concentrated sodium borate solutions at 277 and 317°C. Journal of Solution Chemistry, 24, 409-438.

Wolery, T.W., Xiong, Y.-L., and Long, J. (2010) Verification and Validation Plan/Validation Document for EQ3/6 Version 8.0a for Actinide Chemistry, Document Version 8.10. Carlsbad, NM: Sandia National laboratories. ERMS 550239.

Wood, S.A., Palmer, D.A., Wesolowski, D.J. and Bénézeth, P.A.S.C.A.L.E. (2002) The aqueous geochemistry of the rare earth elements and yttrium. Part XI. The solubility of $Nd(OH)_3$ and hydrolysis of Nd^{3+} from 30 to 290°C at saturated water vapor pressure with in-situ pHm measurement. *Water–rock interactions, ore deposits, and environmental geochemistry: a tribute to David Crerar, Special Publication*, *7*, pp.229–256.

Xiong, Y.-L. (2008) Thermodynamic properties of brucite determined by solubility studies and their significance to nuclear waste isolation. Aquatic Geochemistry, 14, 223–238.

Xiong, Y.-L. (2011) WIPP Verification and Validation Plan/Validation Document for EQ3/6 Version 8.0a for Actinide Chemistry, Revision 1, Document Version 8.20. Supersedes ERMS 550239. Carlsbad, NM. Sandia National Laboratories. ERMS 555358.

Xiong, Y.-L. (2017) Solution Chemistry for Actinide Borate Species to High Ionic Strengths: Equilibrium Constants for $AmHB_4O_7^{2+}$ and $AmB_9O_{13}(OH)_4$(cr) and Their Importance to Nuclear Waste Management. MRS Advances, 2, 741–746.

Xiong, Y.-L., Domski, P.S. (2016) "Updating the WIPP Thermodynamic Database, Revision 1, Supersedes ERMS 565730." Carlsbad, NM: Sandia National Laboratories. ERMS 566047.

Xiong, Y.-L., and Lord, A.C.S. (2008) Experimental investigations of the reaction path in the $MgO–CO_2–H_2O$ system in solutions with ionic strengths, and their applications to nuclear waste isolation. Applied Geochemistry, 23, 1634–1659.

Xiong, Y.-L., Deng, H.-R., Nemer, M., and Johnsen, S. (2010) Experimental determination of the solubility constant for magnesium chloride hydroxide hydrate ($Mg_3Cl(OH)_5·4H_2O$), phase 5) at room temperature, and its importance to nuclear waste isolation in geological repositories in salt formations. Geochimica et Cosmochimica Acta, 74, 4605–4611.

Xiong, Y., Kirkes, L. and Westfall, T. (2013) Experimental determination of solubilities of sodium tetraborate (borax) in NaCl solutions, and a thermodynamic model for the $Na-B(OH)_3-Cl-SO_4$ system to high-ionic strengths at 25°C. American Mineralogist, 98, 2030–2036.

Xiong, Y., Kirkes, L., Knox, J. and Marrs, C. (2017) Experimental determination of solubilities of sodium polyborates in $MgCl_2$ solutions: solubility constant of di-sodium hexaborate tetrahydrate, and implications for the diagenetic formation of ameghinite. The Canadian Mineralogist, 55, 1001–1008.

Xiong, Y., Kirkes, L., Knox, J., Marrs, C. and Burton, H. (2018) Experimental determination of solubilities of magnesium borates: Solubility constants of boracite [$Mg_3B_7O_{13}Cl$(cr)] and aksaite [$MgB_6O_7(OH)_6$•$2H_2O$ (cr)]. Chemical Geology, 483, 254–260.

Yang, Q. (1989) Borate deposits in Qaidam Basin. Acta Sedimentologica Sinica, 7(2), 117–124 (in Chinese with English abstract).

Yang, S. (1991) Saline deposits and minerals of salt lakes in Qinghai-Xizang plateau. Journal of Lake Sciences 3(1), 1–10 (in Chinese with English abstract).

Yang, S. and Zheng, X. (1985) The components of the saline lake in Xizang and approach to their origin. Chinese Journal of Oceanology and Limnology, 3(2), 251–264.

Yeh, D.-N. (1965) Structure of Kurnakovite. Scientia Sinica, 14(7), p.1086.

Yuan, Y.-L., Tang, X.-M., He, Y.-J., (1993) Syntheses and luminescence properties of kurnakovite. Journal of Mineralogy and Petrology, 18(4), 50–55 (in Chinese with English abstract).

Zheng, M. and Liu, W. (1982) The discovery of a lithium-rich magnesian borate deposit in Xizang (Tibet) Di Zhi Lun Ping = Geological Review. 28(3), 263–266 (in Chinese with English abstract).

Zheng, M. and Liu, X. (2009) Hydrochemistry of salt lakes of the Qinghai-Tibet Plateau, China. Aquatic Geochemistry, 15, 293–320.

Zheng, M.P., Qi, W. and Yuan, H.R. (2005) Characteristics of salt lake boron deposits and magnesium borate deposits of the Qinghai-Tibet Plateau, China. In Jingwen Mao, Frank P. Bierlein (eds.) Mineral Deposit Research: Meeting the Global Challenge. Proceedings of the Eighth Biennial Society for Geology Applied to Mineral Deposits Meeting, Beijing, China, 18 - 21 August, 2005, 8(2), 1123–1125. Springer Berlin Heidelberg.

Zhou, B., Michaelis, V.K., Pan, Y., Yao, Y., Tait, K.T., Hyde, B.C., Wren, J.E., Sherriff, B.L. and Kroeker, S. (2012a) Crystal structure refinements of borate dimorphs inderite and kurnakovite using ^{11}B and ^{25}Mg nuclear magnetic resonance and DFT calculations. American Mineralogist, 97, 1858–1865.

Zhou, Y,-Q., Fang, C.-H., Fang, Y., Zhu, F.-Y,, Song, T. and Xu, S. (2012b) Structure of aqueous sodium metaborate solutions: X-ray diffraction study. Russian Journal of Physical Chemistry A, 86, 1236–1244.

Zhou, Y., Higa, S., Fang, C., Fang, Y., Zhang, W. and Yamaguchi, T. (2017) $B(OH)_4^-$ hydration and association in sodium metaborate solutions by X-ray diffraction and empirical potential structure refinement. Physical Chemistry Chemical Physics, 19, 27878–27887.

Table 1. Experimental results of indirect precipitation of kurnakovite from 1.0 mol•kg^{-1} $MgCl_2$ + 1.0 mol•kg^{-1} NaCl solutions at 22.5 ± 0.5 ^{o}C.

Experimental No.	Experimental Duration (day)	pH_m*	Total magnesium molality, $m_{\Sigma Mg}$, mol•kg^{-1}	Total boron molality, $m_{\Sigma B}$, mol•kg^{-1}	Total sodium molality, $m_{\Sigma Na}$, mol•kg^{-1}	Total chloride molality, $m_{\Sigma Cl}$, mol•kg^{-1}
SYN-Boracite-2	957	8.15	1.112	1.199	1.14	3.083
	1204	8.25	1.125	1.220	1.00	3.054
	1266	8.16	1.130	1.180	1.13	3.016
	1289	8.18	1.138	1.233	1.14	3.072
	1322	8.14	1.130	1.197	N/A	3.055
	1470	8.16	1.146	1.191	N/A	3.137
	1582	8.25	1.167	1.091	1.09	3.094
	1629	8.15	1.049	1.030	1.18	3.028

*pcH values are first calculated based on pH readings and correction factors for $MgCl_2$ solutions from Hansen (2001), and are then converted to pH_m based on the equation from Xiong et al. (2010). As the experimental solutions contain significant amounts of sodium and borate as well as the supporting medium, $MgCl_2$, the pH_m's calculated based on the correction factor for pure $MgCl_2$ might have additional experimental uncertainties. The uncertainties for pH_m by using the correction factor for pure $MgCl_2$ are estimated to be less than ± 0.08 according to the comparison with the correction factors for NaCl used in Xiong (2008) at the ionic strengths of the experiments in this work. In the thermodynamic calculations, the uncertainties include those for pH_m.

Table 2. Experimental results for solubility of borax in Na_2SO_4 solutions at 25 ± 0.5 °C.

Experimental No.	Supporting Medium Na_2SO_4 (molal)	Experimental time (day)	pH_m	Molal total boron concentrations, $m_{\Sigma B}$, in equilibrium with sodium tetraborate
$Nd(OH)_3$-B-0.01SO_4-1	0.010	454	9.21	0.529
$Nd(OH)_3$-B-0.01SO_4-2	0.010	454	9.22	0.518
$Nd(OH)_3$-B-0.1SO_4-1	0.10	454	9.08	0.420
$Nd(OH)_3$-B-0.1SO_4-2	0.10	454	9.07	0.407
$Nd(OH)_3$-B-0.5SO_4-1	0.5	454	8.73	0.226
$Nd(OH)_3$-B-0.5SO_4-2	0.5	454	8.73	0.273
$Nd(OH)_3$-B-1.0SO_4-1	1.0	454	8.55	0.232
$Nd(OH)_3$-B-1.0SO_4-2	1.0	454	8.55	0.230
$Nd(OH)_3$-B-1.5SO_4-1	1.5	454	8.55	0.254
$Nd(OH)_3$-B-1.5SO_4-2	1.5	454	8.55	0.222
$Nd(OH)_3$-B-1.8SO_4-1	1.8	454	8.66	0.231
$Nd(OH)_3$-B-1.8SO_4-2	1.8	454	8.66	0.231
$Nd(OH)_3$-B-0.01SO_4-1	0.010	762	9.22	0.527
$Nd(OH)_3$-B-0.01SO_4-2	0.010	762	9.19	0.536
$Nd(OH)_3$-B-0.1SO_4-1	0.10	762	9.04	0.447
$Nd(OH)_3$-B-0.1SO_4-2	0.10	762	9.04	0.455
$Nd(OH)_3$-B-0.5SO_4-1	0.5	762	8.71	0.253
$Nd(OH)_3$-B-0.5SO_4-2	0.5	762	8.71	0.258
$Nd(OH)_3$-B-1.8SO_4-1	1.8	762	8.63	0.212
$Nd(OH)_3$-B-1.8SO_4-2	1.8	762	8.63	0.208
$Nd(OH)_3$-B-0.5SO_4-1	0.5	791	8.74	0.261
$Nd(OH)_3$-B-0.5SO_4-2	0.5	791	8.73	0.267

DOI: https://doi.org/10.2138/am-2020-7212

$Nd(OH)_3$-B-1.0SO_4-1	1.0	791	8.56	0.224
$Nd(OH)_3$-B-1.0SO_4-2	1.0	791	8.56	0.233
$Nd(OH)_3$-B-1.5SO_4-2	1.5	791	8.56	0.207
$Nd(OH)_3$-B-1.8SO_4-2	1.8	791	8.65	0.203
$Nd(OH)_3$-B-0.01SO_4-1	0.010	811	9.33	0.551
$Nd(OH)_3$-B-0.01SO_4-2	0.010	811	9.23	0.553
$Nd(OH)_3$-B-0.1SO_4-1	0.10	811	9.09	0.463
$Nd(OH)_3$-B-0.1SO_4-2	0.10	811	9.09	0.467
$Nd(OH)_3$-B-0.5SO_4-1	0.5	811	8.74	0.303
$Nd(OH)_3$-B-0.5SO_4-2	0.5	811	8.75	0.296
$Nd(OH)_3$-B-1.0SO_4-1	1.0	811	8.56	0.254
$Nd(OH)_3$-B-1.0SO_4-2	1.0	811	8.57	0.247
$Nd(OH)_3$-B-1.5SO_4-1	1.5	811	8.56	0.227
$Nd(OH)_3$-B-1.5SO_4-2	1.5	811	8.56	0.218
$Nd(OH)_3$-B-1.8SO_4-1	1.8	811	8.65	0.205
$Nd(OH)_3$-B-1.8SO_4-2	1.8	811	8.65	0.215

Table 3. Equilibrium constants at infinite dilution for the equilibrium between boracite and kurnakovite and for the dissolution reaction of kurnakovite at 25°C and 1 bar.

Reaction	$\log_{10} K^0$ [A]
$Mg_3B_7O_{13}Cl(cr) + H^+ + 2B(OH)_4^- + 18H_2O(l) \rightleftharpoons 3MgB_3O_3(OH)_5{\bullet}5H_2O(cr) + Cl^-$	12.83 ± 0.08 (2σ)
$MgB_3O_3(OH)_5{\bullet}5H_2O(cr) = Mg^{2+} + 3B(OH)_4^- + H^+ + H_2O(l)$	–14.11 ± 0.40 (2σ)

[A] The equilibrium constants were calculated based on all of the experimental data tabulated in Table 1. The uncertainty in terms of 2σ includes that for the small extrapolation from 22.5°C to the standard temperature of 25°C.

Table 4. Equilibrium constants at infinite dilution for kurnakovite dissolution at 25°C and 1 bar calculated from the Gibbs free energies from the literature.

Reaction	$\log_{10} K^0$
$MgB_3O_3(OH)_5{\bullet}5H_2O(cr) = Mg^{2+} + 3B(OH)_4^- + H^+ + H_2O(l)$	–17.23 [A]
	–21.16 [B]

Note: Calculated using the estimated ΔG_f^0 values from Li et al. (2000) [A] and Anovitz and Hemingway (2002) [B], consistent with the NBS Thermodynamic Tables (Wagman et al., 1982).

DOI: https://doi.org/10.2138/am-2020-7212

Table 5. Thermodynamic properties of kurnakovite, $MgB_3O_3(OH)_5{\bullet}5H_2O(cr)$, at 25°C and 1 bar. The values recommended by this study are in bold.

Species	ΔH_f^0, kJ•mol^{-1}	ΔG_f^0, kJ•mol^{-1}	S^0 J•mol^{-1}•K^{-1}	References and Remarks
Kurnakovite	–4856	–4272	405	Anovitz and Hemingway (2002) [A]
Kurnakovite	–4813.24 ± 2.46			Li et al. (1997) [B]
Kurnakovite	–4831.81	–4249.79	411.85	Li et al. (2000); Entropy calculated in this work [C]
Kurnakovite	**–4813.24 ± 2.46**	**–4231.95 ± 2.29**	**414.31 ± 0.9**	This work [D]

[A] All parameters were estimated.
[B] Enthalpy was experimentally determined.
[C] All parameters were estimated. Gibbs free energy of formation and enthalpy of formation were calculated using the group contribution method of Li et al. (2000). Entropy was calculated internally with the Gibbs-Helmholtz equation by this work from the estimated enthalpy and Gibbs free energy.
[D] Enthalpy is the experimental value of Li et al. (1997) determined using the calorimetric method. Gibbs free energy was computed from the experimentally determined equilibrium constant from this work. Entropy was calculated from the experimental enthalpy of Li et al. (1997) and the derived Gibbs free energy from the experimental equilibrium constant of this work.

Table 6. The revision of the thermodynamic model for the Na–$B(OH)_3$–SO_4 system in Xiong et al. (2013) based on experimental solubility data of borax in Na_2SO_4 solutions at 25°C presented in this work

Pitzer Mixing Parameters and Interaction Parameters Involving Neutral Species				
Species, *i*	Species, *j*	Species, *k*	θ_{ij} or λ_{ij}	Ψ_{ijk} or ζ_{ijk}
$B(OH)_4^-$	SO_4^{2-}		0.17 ± 0.03 (Xiong et al. 2013)	
$B(OH)_4^-$	SO_4^{2-}		–0.00562 ± 0.0026 (P.W.)	
$NaB(OH)_4(aq)$	Na^+		0.093 ± 0.005	
$B_4O_5(OH)_4^{2-}$	SO_4^{2-}	Na^+		0.1 ± 0.2 (Xiong et al., 2013)
$B_4O_5(OH)_4^{2-}$	SO_4^{2-}	Na^+		0.00174 ± 0.0012 (P.W.)
Equilibrium Constants for Solubility and Complex Formation Reactions				
Reaction			log *K* or log β_1 at 25 °C unless otherwise noted	
$Na_2B_4O_7{\bullet}10H_2O^A \rightleftharpoons 2Na^+ + 4B(OH)_4^- + 2H^+ + H_2O$			–24.80 ± 0.10 (2σ) (Xiong et al., 2013)	
$Na^+ + B(OH)_4^- \rightleftharpoons NaB(OH)_4(aq)$			0.25 ± 0.01	

P.W.: present work.
[A]: The structural formula for borax is $Na_2B_4O_5(OH)_4{\bullet}8H_2O$, which is same as its chemical formula that was used in Xiong et al. (2013), $Na_2B_4O_7{\bullet}10H_2O$.

DOI: https://doi.org/10.2138/am-2020-7212

Table 7. A comparison of the experimental invariant solution compositions for the assemblage of Halite (NaCl) + Nahcolite ($NaHCO_3$) + Borax ($Na_2B_4O_7 \cdot 10H_2O$ or $Na_2B_4O_5(OH)_4 \cdot 8H_2O$ as its structural formula) with the values predicted by various models at 25°C.

Elemental Concentrations, $mol \cdot kg^{-1}$	Experimental data [B]	FW86	Xiong et al. (2013)	Re-calibrated Model (Present Work)
B(III)	0.199	0.237	0.176	0.195
Na(I)	6.11	6.33	6.30	6.30
Cl(-I)	5.90	6.00	6.01	6.01
C(IV), TDIC [A]	0.107	0.214	0.208	0.209

[A] TDIC, total dissolved inorganic carbon, as HCO_3^-/CO_3^{2-}
[B] 20°C; from Teeple (1929).

Table 8. A comparison of the experimental solution compositions for the assemblage of Borax ($Na_2B_4O_7 \cdot 10H_2O$ or $Na_2B_4O_5(OH)_4 \cdot 8H_2O$ as its structural formula) + Sodium Pentaborate ($NaB_5O_8 \cdot 5H_2O$) with the values predicted by various models at 25°C.

Elemental Concentrations, $mol \cdot kg^{-1}$	Experimental data [A]	FW86	Xiong et al. (2013)	Re-calibrated Model (Present Work)
B(III)	4.20	5.33	4.21	4.21
Na(I)	1.03	1.36	0.972	0.972

[A] 24°C; from Teeple (1929).

Table 9. Predicted distributions of borate species for the assemblage of borax and mirabilite by using the model in Xiong et al. (2013) and the re-calibrated model in this work

Borate species	Model in Xiong et al. (2013)		Re-calibrated model	
	molality	log a_i	molality	log a_i
$B(OH)_3(aq)$	0.04588	-1.4905	0.050379	-1.4482
$B(OH)_4^-$	0.032386	-1.8985	0.039938	-1.9443
$NaB(OH)_4(aq)$	0.020311	-1.3760	0.018332	-1.4180
$B_3O_3(OH)_4^-$	0.0071235	-3.0793	0.0079010	-3.0398
$B_4O_5(OH)_4^{2-}$	0.0016022	-4.2857	0.0080894	-4.2917
ΣB	0.12606		0.16471	

Figure Captions

Figure 1. XRD patterns of the solid phases from the experiments. The vertical lines in pink, green and blue are the reference peaks of boracite, kurnakovite, and borax, respectively. All of the reference peaks are from the database of the International Centre for Diffraction Data, ICDD. a. The XRD pattern in comparison with those of boracite and borax; b. the XRD pattern in comparison with those of kurnakovite and borax.

Figure 2. Variations of the total boron, chloride, magnesium and sodium concentrations as a function of run duration.

Figure 3. A comparison of experimental solubility data of borax in Na_2SO_4 solutions at 25°C with the values predicted by using various models.

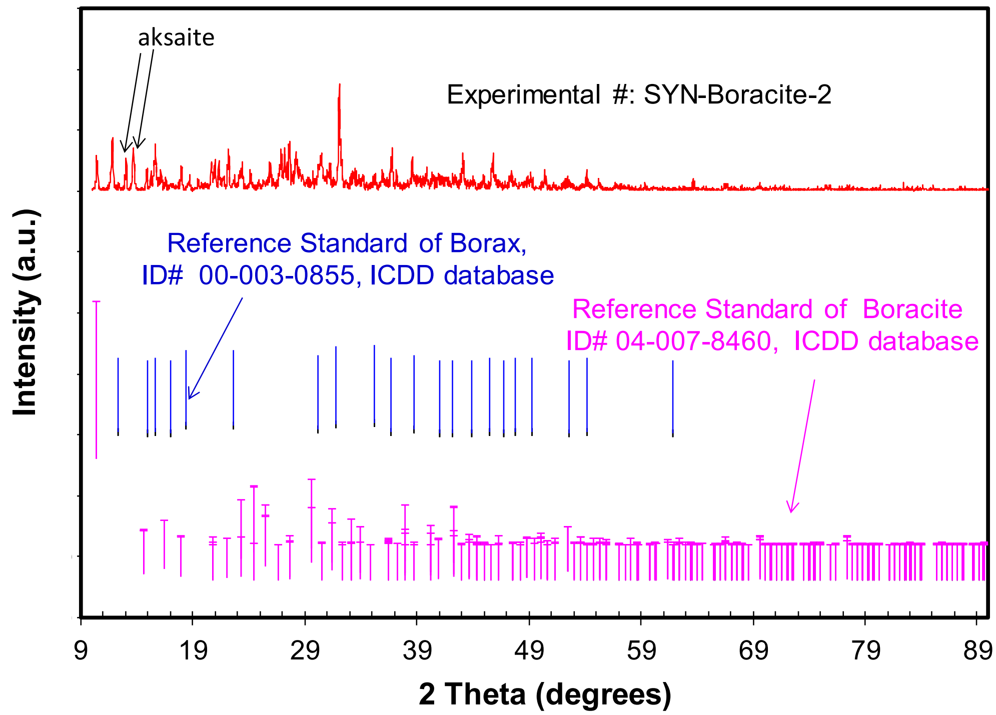
aksaite
Experimental #: SYN-Boracite-2
Reference Standard of Borax,
ID# 00-003-0855, ICDD database
Reference Standard of Boracite
ID# 04-007-8460, ICDD database
Intensity (a.u.)
9
19
29
39
49
59
69
79
89
2 Theta (degrees)

Figure 1a.

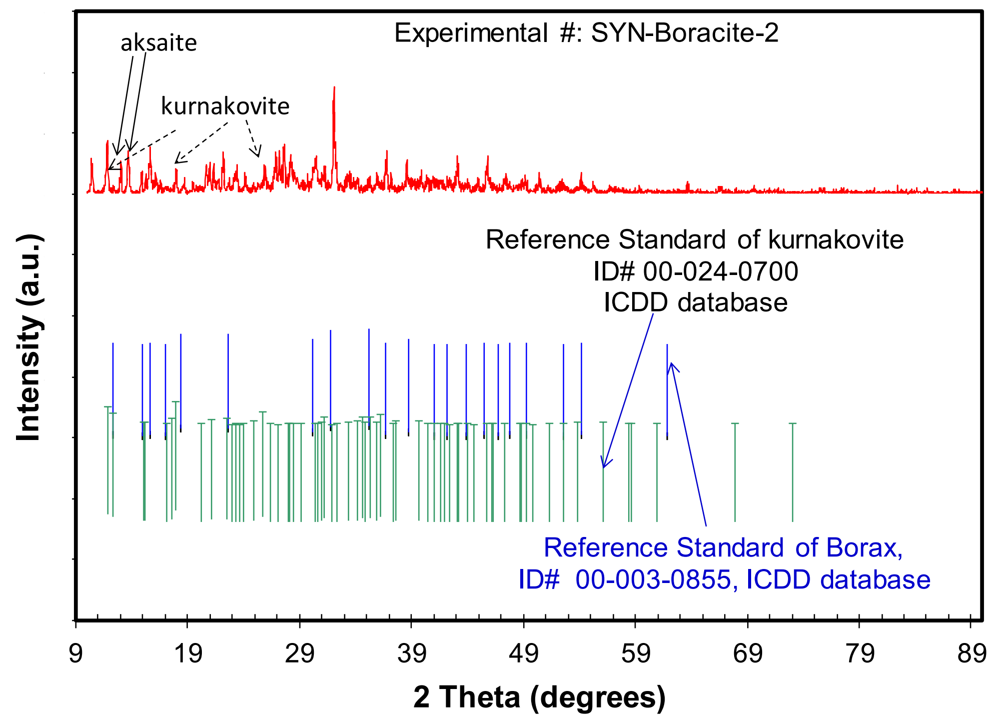
Experimental #: SYN-Boracite-2
aksaite
kurnakovite
Reference Standard of kurnakovite
ID# 00-024-0700
ICDD database
Reference Standard of Borax,
ID# 00-003-0855, ICDD database
Intensity (a.u.)
9
19
29
39
49
59
69
79
89
2 Theta (degrees)

Figure 1b.

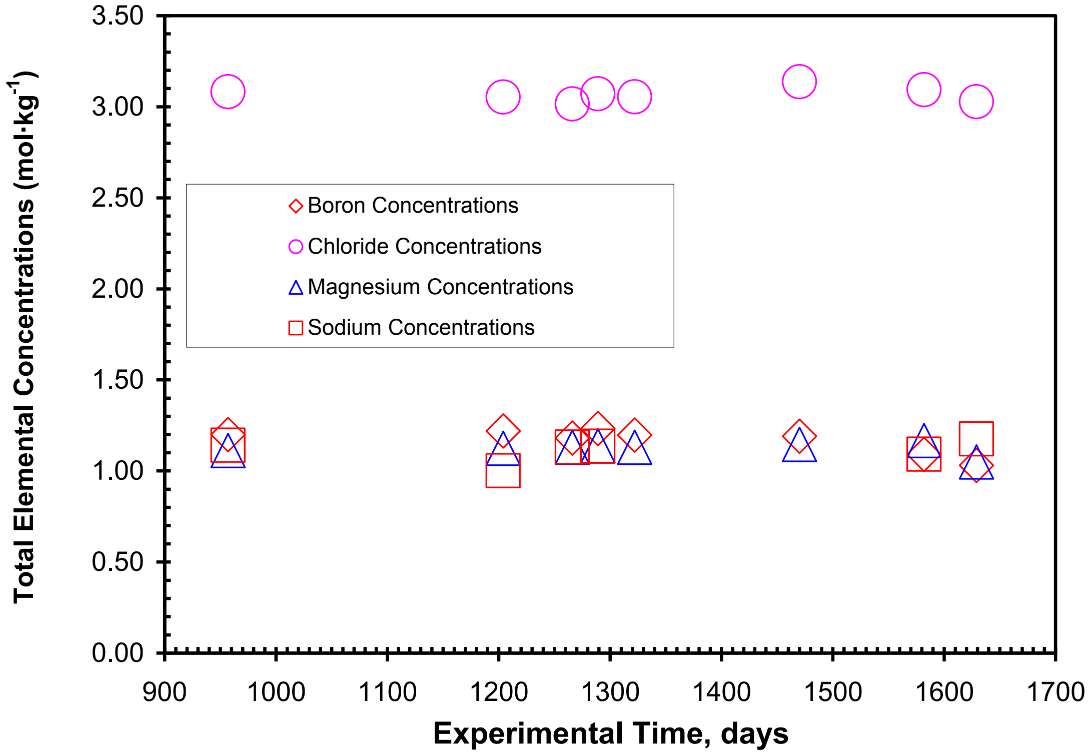
Total Elemental Concentrations (mol·kg⁻¹)
3.50
3.00
2.50
2.00
1.50
1.00
0.50
0.00
900
1000
1100
1200
1300
1400
1500
1600
1700
Experimental Time, days
Boron Concentrations
Chloride Concentrations
Magnesium Concentrations
Sodium Concentrations

Figure 2.

DOI: https://doi.org/10.2138/am-2020-7212

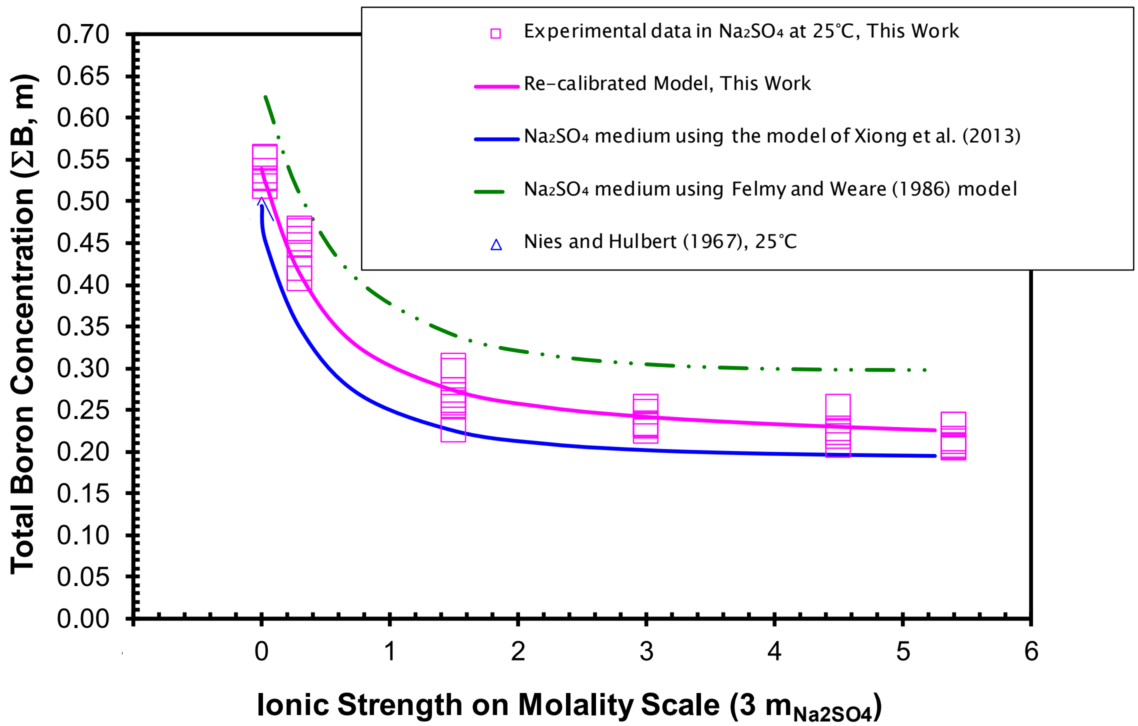

Figure 3.